Dynamic Behaviour in Enzyme-Polymer Surfactant Hydrogel Films

Kamendra P. Sharma,[1] Robert Harniman,[2] Thomas Farrugia[1], Wuge Briscoe,[3] Adam W. Perriman,[4] and Stephen Mann[1]*

[1]Centre for Organized Matter Chemistry and Centre for Protolife Research, School of Chemistry, University of Bristol, BS8 1TS, United Kingdom.

[2]Electron and Scanning Probe Microscopy Unit, School of Chemistry, University of Bristol, BS8 1TS, United Kingdom.

[3]School of Chemistry, University of Bristol, BS8 1TS, United Kingdom.

[4]School of Cellular and Molecular Medicine, University of Bristol, BS8 1TD, United Kingdom.

Dynamic biomaterials define a class of intelligent biostructures that respond to chemical or physical stimuli associated with changes in solvation, pH, ionic strength, molecular recognition, temperature, sound, light, and electric/magnetic fields.[1-3] Intelligent hydrogels form a sub-type of dynamic biomaterials that are receiving considerable attention in fields such as tissue engineering,[4-7] drug delivery,[8-10] food and pharmaceutical industries,[11] robotic actuators,[12] and microfluidics[13] due to their ability to hold water and provide a controllable viscoelastic mechanical response to various external stimuli. Hydrogels with metamaterial-like properties are also being developed, for example for ultrasonic acoustic applications.[14] In general, intelligent hydrogels are fabricated from synthetic polymers, and there are relatively few examples of biomolecules such as DNA and proteins[15] being exploited as dynamic biomaterials or soft metamaterials[16] even though the fabrication of protein/peptide hydrogels is a burgeoning research field.

In principle, proteins offer an attractive route to novel dynamic biomaterials as the chemical accessibility of functional groups at the biomolecule surface provides a route to controlling hydrogel interconnectivity and hence tailoring the viscoelastic response to external stimuli.[17] Such materials are in high demand due to their biocompatibility and biodegradability,[18] and specific relevance to advances in bionanotechnology[20] and medicine.[21] Furthermore, assembling proteins into thin hydrogel films is of major interest for

membrane and sensing applications. However, most examples reported in literature involve hydrogel films comprising structural proteins such as elastin,[22] collagen,[23] silk fibroin,[24] and food proteins (zein, wheat gluten, soy protein),[25] rather than functional proteins (enzymes) with intact globular architecture and chemical activity.[18,26,27] And significantly, studies on protein-based films that show dynamic metamaterial-like responses towards different solvents remain elusive.

Herein we show the first example of dynamical metamaterial-like properties in biofunctionalized hydrogel films fabricated from protein/enzyme-polymer surfactant nanoconjugates. Recently, we described a generic method for the hierarchical self-assembly of protein-polymer surfactant bionano-conjugates into self-standing, enzymatically active hybrid films via a three-step process involving: (a) nano-conjugate synthesis by electrostatically coupling of poly(ethylene glycol) 4-nonylphenyl 3-sulfopropyl ether (C_9H_{19}-C_6H_4-$(OCH_2CH_2)_{19}O(CH_2)_3SO_3^-$ (**S1**)) to cationized derivatives of proteins such as alkaline phosphatase ([cALP-**S1**]), myoglobin ([cMb-**S1**]), glucose oxidase ([cGOx-**S1**]), enhanced green fluorescent protein ([cEGFP-**S1**]), and ferritin [cFn-**S1**] at a charge ratio of approximately 2:1; (b) nanocluster assembly via self-aggregation of the protein-polymer surfactant conjugates; and (c) film formation by capillary-induced assembly of the nanoclusters into micron-sized particles followed by cross-linking in the presence of glutaraldehyde vapour and air drying.[28] In this paper, we demonstrate that self-standing protein/enzyme-polymer surfactant films prepared as described above exhibit unusual dynamical behaviours when exposed to different solvents and liquid/gas interfaces. A solid-to-hydrogel transition occurs on hydration of the hybrid films, which in turn can be utilized for facilitating enzyme reactions or sequestering hydrophilic dye molecules. Moreover, the hydrated protein-polymer surfactant films display an unusual auto-spreading/self-folding response when transferred across the water/air interface. Our results indicate that the biofunctionalized films behave as soft solids when immersed in water and as a quasi-liquid phase in air and non-aqueous environments. These properties originate from the partially crosslinked hierarchical internal structure and are attributed to the low elastic energy required for deformation of the hydrogel-like phase and the role of surface tension in determining film morphology. Overall, our observations provide a step towards the fabrication of novel thin films based on solvent-dependent metamaterials that exhibit hierarchical structure, soft solid/hydrogel transitions, bio-functionality and dynamical responses leading to auto-spreading and self-folding behaviours.

Cross-linked protein-polymer surfactant films were fabricated from a range of bionano-conjugates using a multiple step hierarchical self-assembly process.[28] (see **Experimental** and **Supplementary Information**, **Figure S1**). Significantly, the dry films, which were hard, brittle and exhibited high modulus values,[28] displayed considerable levels of hydrophilicity. Placing a droplet of water onto a dry [cALP-**S$_1$**] film resulted in rapid swelling to produce extensive surface wrinkling and delamination of the film from the bottom of the petri dish (**Figure 1a**, Supplementary Information, **Movie S1**). Typically, a self-standing film, *ca*. 100 μm in thickness, showed an approximately 30% increase in diameter when hydrated (Supplementary Information, **Figure S2**). When saturated with water, the dry films became highly swollen with a water content of *ca.* 80 wt% (TGA, **Figure S3**), corresponding to a volume % of *ca.* 85%. The rheological properties of the cross-linked hydrated [cALP-**S$_1$**] films were determined from frequency sweep measurements, which gave an elastic modulus (G′) of *ca.* 2.1 x 10^3 Pa, consistent with a soft material. The elastic modulus exceeded the viscous modulus (G″) by about an order of magnitude over the entire experimental frequency range of 0.1-100 rad s^{-1} (**Figure 1b,** Supplementary Information, **Figure S4**), indicating an overriding elastic response for small strain values that was consistent with a soft interconnected network structure. Significantly, the elastic and viscous moduli showed a weak frequency dependence with $G' \sim \omega^{0.07}$ and $G'' \sim \omega^{0.12}$, and tan δ = G″/G′ was essentially frequency-independent. These properties were typical of a hydrogel phase.[29] Similar experiments using hydrated [cALP-**S$_1$**] films that were cross-linked by adding 5 w/w% glutaraldehyde in solution rather than glutaraldehyde vapour to an evaporating solution of the protein-polymer surfactant nanoclusters revealed an increased G′ value of *ca.* 1.07 x 10^4 Pa and a minimal frequency dependence of G′ and G″, suggesting that the solution-crosslinked films were also hydrogels (Supplementary Information, **Figure S5**)

To gain further mechanistic understanding on how hydrogel formation and swelling occurred in the hydrated cross-linked protein-polymer surfactant films we undertook a series of AFM and SAXS studies to elucidate the mesoscale and nanoscale structure of the dry samples as well as films soaked in a range of solvents. Atomic force microscopy (AFM) investigations, independently utilising both tapping mode and PeakForce feedback controls, showed a significant increase in the size of [cALP-**S$_1$**] nanoclusters from average values of 18 ± 2 to 52 ± 4 nm for the dry and wet films, respectively (**Figure 2a-c**). A similar degree of nanocluster swelling was also observed in the corresponding dissipation images **(**Supplementary Information, **Figure S6a**), and in tapping mode images of dry and hydrated

films of [cGOx-**S₁**], which consisted of elongated aggregates 17 ± 2 x 23 ± 2 and 42 ± 3 x 92 ± 11 nm, respectively (**Figure S6b**). SAXS profiles of dry and wet [cALP-**S₁**] films showed changes in the mesoscale spacings between individual protein-polymer surfactant nanoconjugates that were commensurate with swelling of the wet films. The dry [cALP-**S₁**] film showed a broad peak centred at 0.077 $Å^{-1}$, which shifted towards a lower q value of 0.066 $Å^{-1}$ upon introduction of the cross-linked film into water (**Figure 2d**). As the correlation/structure factor peak was absent in the scattering profile of a *ca.* 1.5 mg mL^{-1} dilute aqueous solution of [cALP-**S₁**], this profile was utilised to provide a form factor ($F(q)$) for the nanoconjugate, which was fitted using a core-shell model consisting of an ALP protein core and **S₁** shell with size and thickness of 4.84 and 1.51 nm, respectively, and polydispersity of 0.19 (see Supplementary Information, **Figure S7** for details). Apparent structure factors, $S_{app}(q)$, were calculated for the dry and hydrated [cALP-**S₁**] films (**Figure 2e**) and fitted to obtain the peak position using an interference function for densely packed systems, $S_{app}(q) = A/[1 + B \times F(q)]$, where A is a constant, and B the packing factor. Using this approach, the average size of the dry protein-polymer surfactant core-shell nanoconjugate was determined as 6.2 nm, which was very similar to the value of 6.35 nm obtained from the form factor data. Moreover, hydration of [cALP-**S₁**] film increased the $S_{app}(q)$ peak to a value of 7.5 nm, consistent with the swelling of the polymer surfactant corona observed by AFM.

We also undertook a series of SAXS and WAXS experiments on dry [cALP-**S₁**] films that were immersed in various solvents to assess the swelling response across the nano- and mesosopic length scales. SAXS profiles recorded on films immersed in brine or ethanol (polarity index = 5.2; *cf.* water = 10.2) were very similar to those recorded on the hydrated films (Supplementary information, **Figure S8**), suggesting that the swelling properties associated with hydrogel formation in the cross-linked films were primarily driven by polar and not electrostatic interactions, presumably involving the poly(ethylene glycol) domains of the polymer surfactant molecules. In contrast, minimal changes in the SAXS data were observed when a dry [cALP-**S₁**] film was dipped in toluene (polarity index = 2.4; **Figure 2d, e**), whilst films immersed in iso-octane (polarity index = 0.01) showed a slight deswelling of the cross-linked matrix (correlation peak at 0.084 $Å^{-1}$; $S_{app}(q)$-derived d-spacing = 5.9 nm (**Figure 2 d, e**). Corresponding WAXS profiles showed a decrease in the polymer surfactant alkyl-alkyl chain d-spacing from 0.440 nm in the dry film to 0.338 nm in the presence of water, whilst immersion in toluene or iso-octane gave an increase in the alkyl-alkyl d-spacing to 0.447 or 0.449 nm, respectively, due to solvation of the alkyl chains (**Figure 2f**).

Taken together, the X-ray scattering and AFM data indicated that water-induced mesoscale expansion of the protein-polymer surfactant nanoclusters within the cross-linked matrix was responsible for hydrogel formation and the concomitant swelling observed at the macroscopic level in the protein-polymer surfactant films. Based on these observations, we utilised the hydration-induced soft solid to hydrogel film transition as a mode of activating a water-mediated enzymatic switch for a microemulsion-based biochemical transformation (**Figure 3a)**. For this, *p*-nitrophenyl phosphate (*p*NPP) was encapsulated into the water micro-droplets of a transparent iso-octane microemulsion containing sodium bis-2-ethylhexyl sulphosuccinate (AOT) prepared at a [H_2O/AOT] molar ratio of *ca.* 100, and a dry and folded [cALP-$\mathbf{S_1}$] film immersed into the dispersion. Within 1 min, the film unravelled and swelled, and the microemulsion became transparent, suggesting that hydration of the [cALP-$\mathbf{S_1}$] film was associated with extraction of water molecules from the microemulsion droplets (**Figure 3b).** This was confirmed by DLS measurements (**Figure 3c**), which showed a change in the size of the microemulsion droplets from 88.9±45.7 nm to 1.85±0.23 nm before and 10 minutes after immersion of the film, respectively. In addition, the hydrated film turned bright yellow and fluffy in texture over a period of 10-15 minutes (**Figure 3b** and Supplementary Information, **Figure S9)**. Development of the yellow colouration, which was monitored by measuring the increase in absorbance at 410 nm at different time periods(**Figure 3d**), was attributed to the onset of ALP-mediated conversion of *p*NPP to *p*-nitrophenyl phenolate (*p*NP) associated with *in situ* formation of the hydrated enzyme-polymer surfactant hydrogel film. To confirm that the sponge-like film was absorbing the microemulsion water droplets, we replaced the entrapped *p*NPP substrate with a water-soluble rhodamine B dye, and inserted dry pieces of [cALP-$\mathbf{S_1}$] film into the pink microemulsion. The hydrated film became progressively red in colour as the microemulsion became decolourized (**Figure 3e** and Supplementary information, **Figure S10**), indicating that the transfer of water to the enzyme-polymer surfactant film was accompanied by uptake of the dye molecules.

Transfer of the hydrated cross-linked protein-polymer surfactant films across a water/air interface gave rise to an unusual reversible self-folding and auto-spreading behaviour. When immersed in water, the intact films were unfolded and highly spread, but when held between tweezers and lifted out of the water phase, the segment exposed to the air immediately crumpled into a compact, folded ball, whilst regions of the film in the water remained in a highly extended conformation (**Figure 4** and Supplementary Information, **Figures S11, S12**). Folding of the hydrogel film was complete as soon as the entire protein-

polymer surfactant film was lifted out of the water. On re-immersion in the water phase, the folded film unravelled instantaneously into the original shape without loss of structure (**Figure 4** and Supplementary Information, **Figures S11, S12** and **Movie S2**). In general, self-folding and auto-spreading behaviour were dependent on film thickness. For example, films cross-linked using 5 wt.% vapour glutaraldehyde exhibited a critical thickness (t_c) of 805.7±134.3 μm, above which they did not self-fold when transferred across the water/air interface (Supplementary Information, **Figure S16**).

We used the above phenomena to transfer the hydrated protein-polymer surfactant films without loss of structure or morphology onto hydrophilic (glass) or hydrophobic (teflon) surfaces (Supplementary Information, **Figure S13**), and to prepare optically transparent thin membranes by mounting the transferred hydrogel films across small apertures (Supplementary Information, **Figures S14**). Significantly, the dry protein-polymer surfactant films did not re-spread when placed into water from the air, but exhibited neutral buoyancy such that they rapidly unfolded once in the water phase, indicating that the folding process was associated with retention of the hydrophilic nature of the cross-linked protein-polymer surfactant network. This was consistent with experiments in which crumpled films prepared as above were immersed into toluene; under these conditions the films remained tightly folded and no auto-spreading was observed (Supplementary Information, **Figure S15** and Supplementary Information, **Movie S3**). However, immersing the toluene-exposed film in water resulted in displacement of the organic solvent and re-established the auto-spreading behaviour.

The above phenomenological observations indicate that the dry cross-linked films are highly hydrophilic and undergo a solid to hydrogel transition on hydration to produce a mechanically elastic soft material with low cohesive energy. As a consequence, the auto-spreading/self-folding behaviour is not a direct consequence of hydration/de-hydration occurring at the water/air interface but is associated with a dramatic collapse of the hydrated films into a compact folded morphology presumably due to the low elastic energy required for crumpling being overwhelmed by the high surface tension. The excluded volume energy associated with crumpling is small for a thin completely spread circular film of radius $R \sim 1$ cm and thickness $t \sim 100$ μm (Föppl-von Kármán number $\sim (R/t)^2 \sim 10^4$ (Ref. 30)), and the elastic energy for the thin sheet to undergo crumpling to a folded state of radius r is $E_{\text{crumpling}} \sim tYR^2(t/r)^{5/3}$ (Ref 31), where $r \sim 1.5$ mm for the folded films described above. The elastic modulus Y of the hydrogel film is given by $Y = 2G(1+\upsilon)$, where G is the shear modulus

obtained from rheology measurements (~ 2.1×10^{3} Pa), and υ the Poisson ratio (transverse stain/axial strain ~ 0.5 for an isotropic incompressible material). Given these values the $E_{\text{crumpling}}$ was estimated to be 6.57×10^{-4} mJ, which is *ca.* two orders of magnitude lower than the calculated interfacial energy gain (~ 4.31×10^{-2} mJ) associated with concealing the highly hydrophilic film surface from the air ($E_{\gamma} \sim \gamma \Delta A$, where γ is the surface tension at the water/air interface, ΔA the difference in surface area between the completely spread and a folded film; see supplementary information for details). Thus, for a thin self-standing film (t ~ 100 μm), the interfacial energy gain readily overcomes the crumpling energy (which opposes deformation) when the film is pulled out of the water, resulting in instantaneous self-folding of the film. In contrast, when the compacted films are re-immersed into water from the air, neutral buoyancy is exhibited by the film and the surface interfacial tension vanishes, resulting in auto-spreading of the film by the overriding elastic energy.

Similar calculations were undertaken for [cALP-**S$_1$**] films with $t \geq t_c$ (t_c ~ 800 nm (experimental), Supplementary Information, **Figure S16**). The values for $E_{crumpling}$ were typically between 10^{-3} and 10^{-2} mJ, which are comparable to E_{γ}, and consistent with the absence of auto-spreading/self-folding behaviour in these materials. Significantly, the theoretical calculations for t_c for 1 cm-sized films gave a critical threshold between 500 and 1000 μm (Supplementary information, **Figure S17**), indicating that the theoretical model and experimental data were in good agreement.

Finally, we used the de Gennes scaling term, $Y \sim kT/\xi^3$ (kT = 4.11×10^{-21} J, ξ = correlation length) to estimate the mesh size between crosslinking points in the biomolecular matrix. The calculation gave a value of $\xi \sim 8.81$ nm, which was in close agreement to size of the hydrated nanoconjugates determined by SAXS (7.86 nm). Thus, the overall elastic property of the films appears to be determined by physical interactions of the order of kT, which drive the hierarchical self-assembly of the nanometer-sized clusters and their subsequent aggregation into micro-particles. As a consequence, the softness (low Y) of the hydrated hydrogel films is underpinned by both the nanoscopic structure and the low cohesive energy of the cross-linked protein-polymer surfactant network.

In conclusion, our results indicate that self-supporting bio-functionalized films exhibiting hierarchical structure and unusual dynamical responses can be readily prepared by self-association and cross-linking of hybrid nanoclusters that are generated *in situ* from the self-assembly of diverse protein-polymer surfactant nano-conjugated building blocks. The

dry films are highly hydrophilic and show a soft solid to hydrogel transition upon hydration that produces swollen hydrogel films, which can be exploited for extracting water-soluble dye molecules from water micro-droplet in oil dispersions, or initiating enzyme-mediated transformations within the cross-linked film. Significantly, an unusual reversible auto-spreading/self-folding response is observed when the water-saturated films are transferred from water into air. The dramatic collapse of the hydrated hydrogel film into a compact folded ball on exposure to air is attributed to the generation and dissipation of a high interfacial energy that is possibly comparable to the air/water surface tension ($\gamma \sim 72$ mJ m^{-2}). Thus, given the viscoelastic nature of the hydrogel films, internalization of the hydrophilic surfaces on exposure to air can occur spontaneously without structural disintegration provided that the elastic energy of the protein-polymer surfactant network is offset by the high surface tension energy. This behaviour is typical of a metamaterial. Our results therefore provide a step towards the development of protein/enzyme-based metamaterials with tunable mechanical properties for potential use as biologically active membranes and soft mechanical switches in diverse areas of bionanotechnology.

Experimental Section

Preparation of protein-polymer surfactant bioconjugates and hybrid films. Native proteins (alkaline phosphatase (ALP), ferritin (Fn), myoglobin (Mb), enhanced green fluorescent protein (EGFP), or glucose oxidase (GOx)) were cationized by covalent coupling of glutamic and aspartic acid residues with 3-dimethylamino propylamine (DMAPA) by addition of N-(3-dimethylaminopropyl)-N′-ethylcarbodiimide hydrochloride to yield cationized alkaline phosphatase (cALP), cationized ferritin (cFn), cationized myoglobin (cMb), cationized enhanced green fluorescent protein (cEGFP), or cationized glucose oxidase (cGO_x). Briefly a 2 mL of 0.2 M solution of DMAPA was adjusted to pH 6 using HCl (6M), after which it was added to a 10 mL solution of 5 mg mL^{-1} of native protein dissolved in MilliQ 18.2 $M\Omega^{-1}$ cm^{-1} water. After this 100 mg of EDC was added to the mixture. The reaction was allowed to proceed overnight, and the pH was adjusted to 6 at hourly intervals for the first 3 hours. This step was followed by dialysis of the cationized protein against MilliQ grade water, with three water changes. Any aggregates that formed during the reaction or dialysis steps were removed by centrifugating the modified proteins at 5000 rpm for 10 mins. Cationization efficiency was determined using MALDI TOF mass spectrometry (Supplementary Information, **Figure S20**) and used to determine the amount of polymer surfactant required to half neutralize the protein surface charge required for nanocluster formation. Formation of the protein-polymer surfactant conjugates was achieved by controlled addition of a 50 mg mL^{-1} solution of $\mathbf{S_1}$ at a steady rate of 100 µL min^{-1} using a syringe pump to a stirred solution of 10 ml of 5-10 g mL^{-1} cationized protein. Formation of the bioconjugates and their spontaneous association into nanoclusters at a 1 : 2 stoichiometry was associated with an increase in solution turbidity.

Films of bioconjugate proteins were produced by dispensing solutions of the bioconjugate nanoclusters into polystyrene petri dishes, after which they were placed in a vacuum desiccator containing a petri dish filled with silica beads and 5 wt.% glutaraldehyde and left overnight to dry and cross-link. Drying was facilitated by application of a 25 mm Hg vacuum to the desiccator. The resulting self-standing, crosslinked films were removed from the petri-dish by the addition of MilliQ grade water, which resulted in swelling of the film and buckling instabilities that resulted in delamination from the polystyrene dish.

Water-in-oil microemulsion experiments:. Typically, 50 mg of solid sodium bis(2-ethylhexyl) sulfosuccinate (AOT) and 200 µL of 100 mM *p*NPP aqueous solution were added to 5 mL of iso-octane (2,2,4-trimethylpentane) to produce water-in-oil microemulsion droplets. The mixture was thoroughly vortexed to form a microemulsion with a molar ratio of $w \approx 100$; (w= $[H_2O]/[AOT]$). Using a linear relationship between the radius of the aqueous droplets (R_w) and w, a theoretical radius of the water pool was calculated as R_w = 15 nm ($0.15w$).[32] A dry and folded [cALP-$\mathbf{S_1}$] film (~ 5mg) was then lowered into the vial containing the microemulsion using tweezers and dephosphorylation of *p*-nitrophenyl phosphate (*p*NPP) to *p*-nitro phenol (*p*NP) was monitored using snapshots from a digital camera over 10-15

minutes. For the dye uptake experiments, the *p*NPP aqueous solution was replaced by 50 µL of 1 mM rhodamine B dye aqueous solution providing a microemulsion with $w \approx 25$ and water pool radius, $R_w = 3.75$ nm.

Acknowledgements

We thank Dr. James Armstrong for the preparation of EGFP. AFM studies were conducted at the Imaging Facility of the School of Chemistry in the University of Bristol.

References:

1. Langer, R.; Tirrell, D. A. *Nature* **2004**, *428*, 487.
2. Lee, K. Y.; Mooney, D. J. *Chem. Rev.* **2001**, *101*, 1869.
3. Lowik, D. W. P. M.; Leunissen, E. H. P.; van den Heuvel, M.; Hansen, M. B.; van Hest, J. C. M. *Chem. Soc. Rev.* **2010**, *39*, 3394.
4. Monzack, E.; Rodriguez, K.; McCoy, C.; Gu, X.; Masters, K. In *Biomaterials for Tissue Engineering Applications*; Burdick, J., Mauck, R., Eds.; Springer Vienna: 2011, p 209.
5. K. Rajagopal and J. P. Schneider, *Curr. Opin. Struct. Biol*., **2004**, *14*, 480.
6. K. Y. Lee and D. J. Mooney, *Chem. Rev.*, **2001**, *101*, 1869
7. M. P. Lutolf and J. A. Hubbell, *Nat. Biotechnol.*, **2005**, *23*, 47.
8. N. A. Peppas, P. Bures, W. Leobandung and H. Ichikawa, *Eur. J. Pharm. Biopharm.*, **2000**, *50*, 27.
9. A. S. Hoffman, *Adv. Drug Delivery Rev.*, **2002**, *54*, 3.
10. R. Langer and N. A. Peppas, *AIChE J.*, **2003**, *49*, 2990.
11. A. A. Apostolov, D. Boneva, E. Vassileva, J. E. Mark and S. Fakirov, *J. Appl. Polym. Sci.*, **2000**, *76*, 2041.
12. Morales, D.; Palleau, E.; Dickey, M. D.; Velev, O. D. *Soft Matter* **2014**, *10*, 1337.
13. D. J. Beebe, J. S. Moore, J. M. Bauer, Q. Yu, R. H. Liu, C. Devadoss and B. H. Jo, *Nature*, **2000**, *404*, 588.
14. (a) B. Garner, T. Cai, Z. Hu., A. Neogi, *Optics Exp.* **2008**, *16*, 19410. (b) S. Ghosh, Y. Chao, T. Cai, Z. Hu, A. Neogi, *J. Phys. D: Appl. Phys.* **2009**, *42*, 135501. (c) B. Garner, T. Cai, M. Kim, Z. Hu, A. Neogi, Appl. Phy. Exp. **2009**, *2*, 075001. (d) Walker, E.; Reyes, D.; Rojas, M. M.; Krokhin, A.; Wang, Z.; Neogi, A. *Appl. Phys. Lett.* **2014**, *105*, 143503.
15. (a) Xing, Y.; Cheng, E.; Yang, Y.; Chen, P.; Zhang, T.; Sun, Y.; Yang, Z.; Liu, D. *Adv. Mater.* **2011**, *23*, 1117. (b) Jonker, A. M.; Löwik, D. W. P. M.; van Hest, J. C. M. *Chem. Mater.* **2012**, *24*, 759.
16. Lee, J. B.; Peng, S.; Yang, D.; Roh, Y. H.; Funabashi, H.; Park, N.; Rice, E. J.; Chen, L.; Long, R.; Wu, M.; Luo, D. *Nat Nano* **2012,** *7* (12), 816-820.
17. van Hest, J. C. M.; Tirrell, D. A. *Chem. Commun.* **2001**, 1897.
18. Banta, S.; Wheeldon, I. R.; Blenner, M. *Annual Review of Biomedical Engineering* **2010**, *12*, 167.
19. Shen, W. In *Biomaterials for Tissue Engineering Applications*; Burdick, J., Mauck, R., Eds.; Springer Vienna: **2011**, p 243.
20. de la Rica, R.; Matsui, H. *Chem. Soc. Rev.* **2010**, *39*, 3499.
21. Bennett, S. L.; Melanson, D. A.; Torchiana, D. F.; Wiseman, D. M.; Sawhney, A. S. *Journal of Cardiac Surgery* **2003**, *18*, 494.

22. (a) Urry D. W. *J. Phys. Chem. B* **1997**, *101*, 1007–11028. (b) Almine, J. F.; Bax, D. V.; Mithieux, S. M.; Nivison-Smith, L.; Rnjak, J.; Waterhouse, A.; Wise, S. G.; Weiss, A. S. *Chem.Soc. Rev.* **2010**, *39*, 3371.
23. Lu, J. T.; Lee, C. J.; Bent, S. F.; Fishman, H. A.; Sabelman, E. E. *Biomaterials* **2007**, *28*, 1486.
24. Prince, J. T., McGrath, K.P., DiGirolamo, C. M., Kaplan, D. L. *Biochemistry* **1991**, *281*, 10879–10885.
25. Dangaran, K.; Tomasula, P.; Qi, P. In *Edible Films and Coatings for Food Applications*; Huber, K. C., Embuscado, M. E., Eds.; Springer New York: **2009**, p 25.
26. Petka, W. A.; Harden, J. L.; McGrath, K. P.; Wirtz, D.; Tirrell, D. A. *Science* **1998**, *281*, 389.
27. (a) King, W. J.; Toepke, M. W.; Murphy, W. L. *Chem. Commun.* **2011**, *47*, 526. (b) Kong, N.; Peng, Q.; Li, H. *Adv. Funct. Mater.* **2014**, *24*, 7310.
28. Sharma, K. P.; Collins, A. M.; Perriman, A. W.; Mann, S. *Adv. Mater.* **2013**, *25*, 2005.
29. Le, X. T.; Turgeon, S. L. *Soft Matter* **2013**, *9*, 3063; Doublier, J.-L.; Choplin, L. *Carbohydr. Res.* **1989**, *193*, 215.; Suriano, R.; Griffini, G.; Chiari, M.; Levi, M.; Turri, S. *J. Mech. Behav. Biomed. Mater.* **2014**, *30*, 339.
30. Vliegenthart, G. A.; Gompper, G. *Nat. Mater.* **2006**, *5*, 216-221.
31. Kramer, E. M.; Witten, T. A. *Phys. Rev. Lett.* **1997**, *78*, 1303.
32. Pileni, M. -P. *Adv. Colloid Interface Sci.* **1993**, *46*, 139.

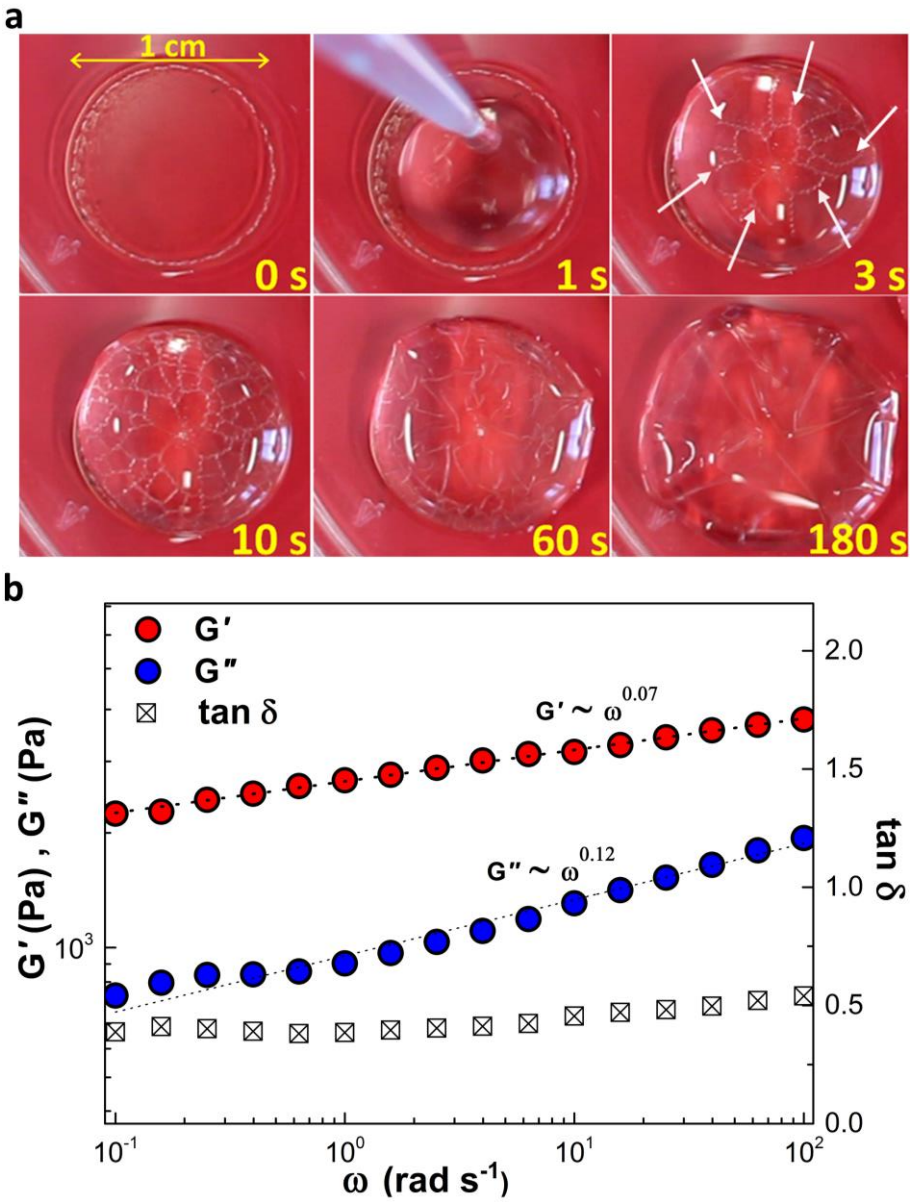

Figure 1: Dynamic metamaterial-like response of functional [cALP-S_1] hybrid films (a) Optical images showing swelling-induced wrinkling (white arrows) in a dry protein-polymer surfactant film on contact with water for various time periods. (b) Rheological responses for a hydrated [cALP-**S_1**] film exhibiting hydrogel properties. Dynamic frequency sweep of a wet [cALP-**S_1**] film over a frequency range of 0.01 to 100 rad s^{-1} and 0.1% strain at 25°C showing the dependence of elastic (G′) and viscous (G″) moduli on frequency**.**

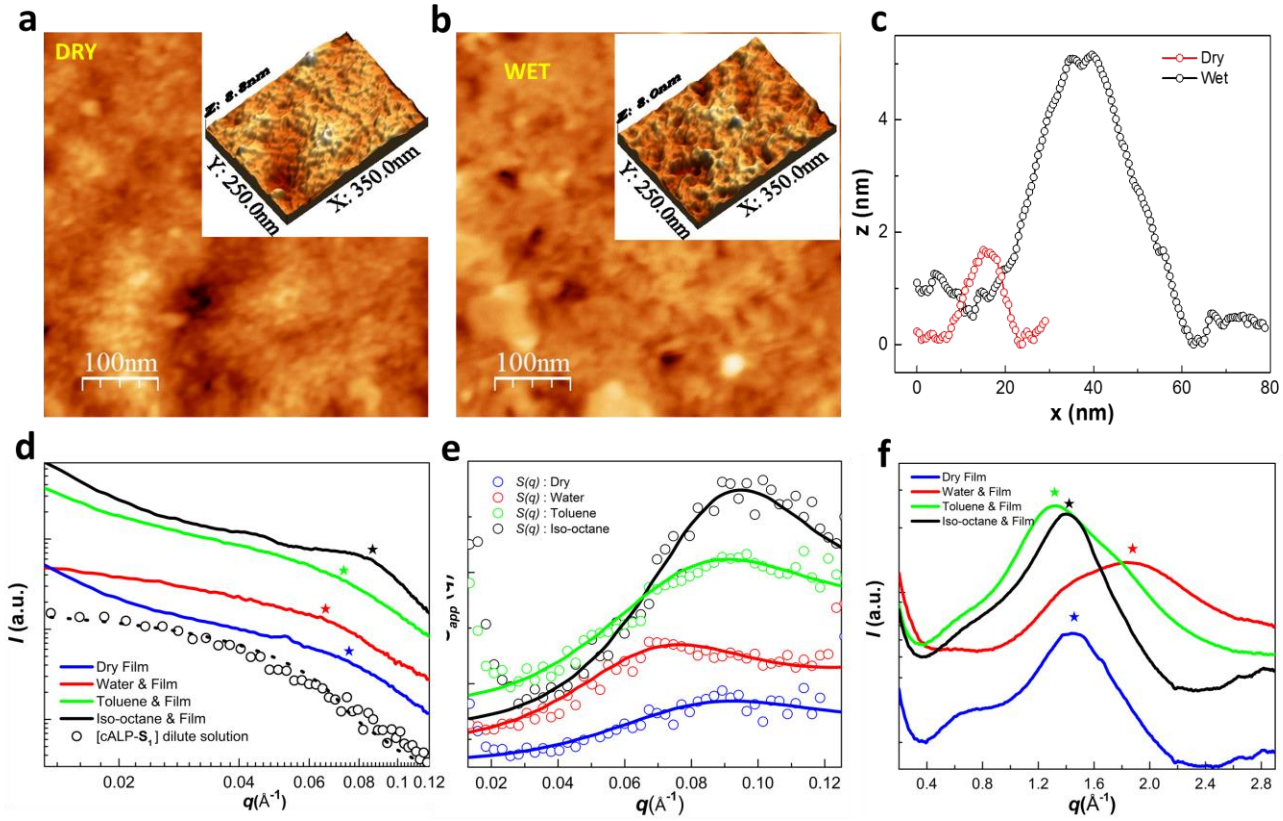

Figure 2: AFM and scattering data for [cALP-S_1] film. (a,b) AFM topography 2D (a, b) and 3D (*insets* in a, and b) images for [cALP-S_1] films in dry (a) and water-saturated (b) states. The topography images indicate that the nanoclusters swell in the presence of water. (c) Representative line profiles averaged over 10 clusters showing increase in nanocluster size from 18 ± 2 nm to 52 ± 4 nm in the dry and hydrated states, respectively. (d) SAXS profiles (solid lines) showing approximate positions of the correlation peaks (asterisks) for a dry film (blue), and films immersed in water (red), toluene (green), or iso-octane (black). Scattering from a dilute aqueous solution of [cALP-S_1] (black circles) and theoretical fit according to a form factor model for a core-shell structure (dashed line) are also shown. (e) Apparent structure factor profiles showing clear shift in the correlation peak in the presence of different solvents. (f) WAXS profiles showing changes in polymer surfactant alkyl-alkyl intermolecular spacing for a dry film and films immersed in various solvents. Colour schemes in (e) and (f) are identical to that shown in (d).

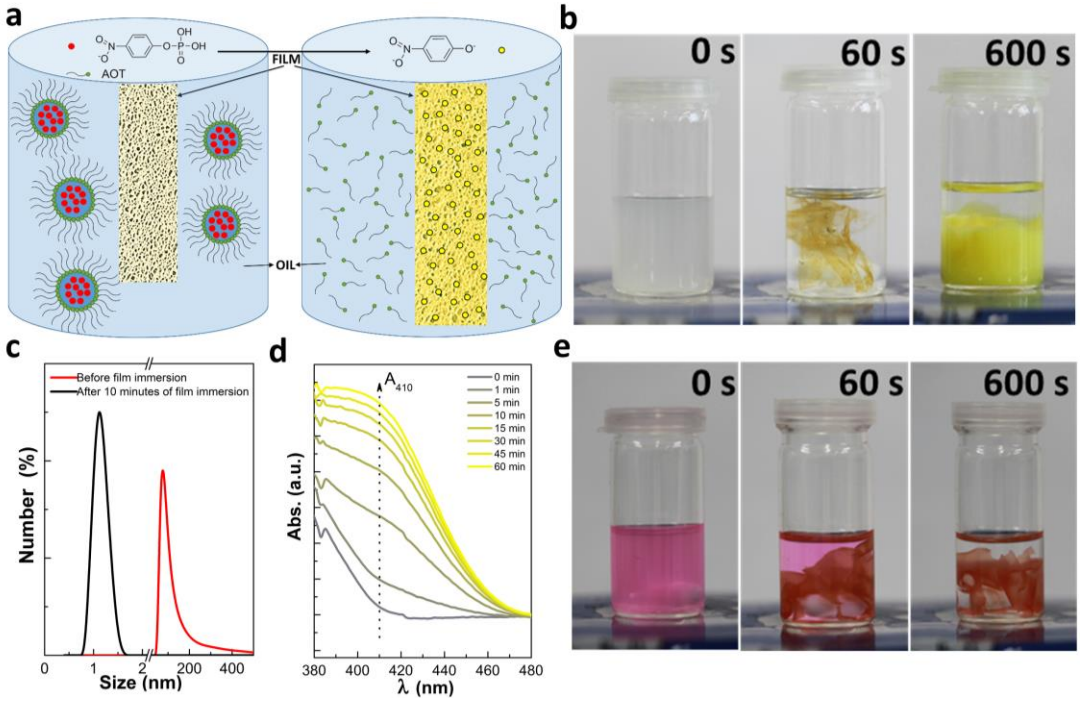

Figure 3: (a) Schematic showing the mechanism of water-triggered enzymatic switch: Left panel shows the *p*NPP substrate as red circles trapped in the aqueous droplets stabilized using AOT in iso-octane. The spongy film shows no swelling response to isooctane, however, upon water absorption accompanied by the uptake of *p*NPP molecules, the film swells (right panel). Enzymatic conversion of the *p*NPP is depicted by the increase in the yellow colour of the film due to accumulation of *p*NP (yellow circles). (b) Photographs of sample tube showing cloudy, water-in-oil AOT-stabilized microemulsion comprising *p*NPP-containing aqueous droplets in iso-octane (t = 0), and same sample tube 60 s (middle) and 600 s (right) after addition of a dry compact globule of folded **[**cALP-**S_1**]**. Yellow coloration in the swollen film is due to formation of the enzyme-mediated product, *p*NP. (c) DLS data showing microemulsion droplet size before (red curve) and 10 minutes after immersion of a **[**cALP-**S_1**]** film (black profile). (d) UV-vis spectra showing increase in absorbance at 410 nm due to formation of *p*NP associated with a thin section of a **[**cALP-**S_1**]** film before (grey) and after immersion for different time periods to a *p*NPP-containing microemulsion at 25°C. (e) Photographs of sample tubes showing time-dependent uptake of rhodamine B by a [cALP-**S_1**] film immersed in a dye-containing water-in-oil microemulsion.

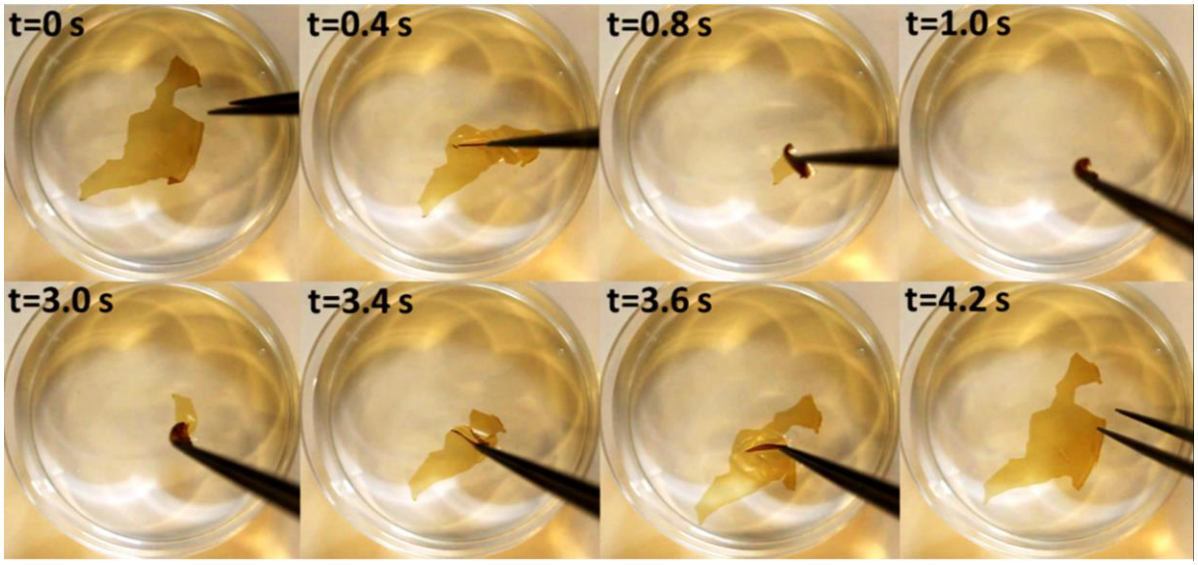

Figure 4: Reversible auto-spreading and self-folding of hydrated protein-polymer surfactant hybrid films induced by transfer across the water/air interface. Time sequence of photographs showing a hybrid [cMb-**S_1**] film initially spread under water (t = 0) followed by removal from the water phase to produce rapid crumpling and compaction of the film in air (t = 0.4 to 1.0 s). Re-immersion (at t = 3.0 s) of the folded film into the water phase results in instantaneous unravelling and re-spreading to its original shape without loss of structural integrity (t = 3.0 to 4.2 s).